Baroclinic Rossby Wave Forcing and Barotropic Rossby Wave Response to Stratospheric Vortex Variability

J. M. CASTANHEIRA

CESAM, Department of Physics, University of Aveiro, Aveiro, Portugal

M. L. R. LIBERATO

Physics Department, University of Trás-os-Montes e Alto Douro, Vila Real, Portugal

L. DE LA TORRE

CESAM, Department of Physics, University of Aveiro, Aveiro, Portugal

H.-F. GRAF

Centre for Atmospheric Science, Geography Department, University of Cambridge, Cambridge, United Kingdom

C. C. DACAMARA

CGUL, IDL, University of Lisbon, Lisbon, Portugal

(Manuscript received 20 June 2008, in final form 15 October 2008)

ABSTRACT

An analysis is performed on the dynamical coupling between the variability of the extratropical stratospheric and tropospheric circulations during the Northern Hemisphere winter. Obtained results provide evidence that in addition to the well-known Charney and Drazin mechanism by which vertical propagation of baroclinic Rossby waves is nonlinearly influenced by the zonal mean zonal wind, topographic forcing constitutes another important mechanism by which nonlinearity is introduced in the troposphere–stratosphere wave-driven coupled variability. On the one hand, vortex variability is forced by baroclinic Rossby wave bursts, with positive (negative) peaks of baroclinic Rossby wave energy occurring during rapid vortex decelerations (accelerations). On the other hand, barotropic Rossby waves of zonal wavenumbers $s = 1$ and 3 respond to the vortex state, and strong evidence is presented that such a response is mediated by changes of the topographic forcing due to zonal mean zonal wind anomalies progressing downward from the stratosphere. It is shown that wavenumbers $s = 1$ and 3 are the dominant Fourier components of the topography in the high-latitude belt where the zonal mean zonal wind anomalies are stronger; moreover, obtained results are in qualitative agreement with the analytical solution provided by the simple topographic wave model of Charney and Eliassen. Finally, evidence is provided that changes of barotropic long ($s \leq 3$) Rossby waves associated with vortex variability reproduce a NAO-like dipole over the Atlantic Ocean but no dipole is formed over the Pacific Ocean. Moreover, results suggest that the nonlinear wave response to topographic forcing may explain the spatial changes of the NAO correlation patterns that have been found in previous studies.

1. Introduction

Since the end of the 1990s, there has been increasing observational and modeling evidence that the stratosphere does not respond passively to tropospheric forcing but instead plays an important role in driving climate and weather variability in the troposphere down to the surface (e.g., Haynes 2005). One of the proposed mechanisms for the way the stratosphere might affect the tropospheric circulation is via Rossby wave propagation. This mechanism includes changes in the upward and meridional wave fluxes that are caused either by

Corresponding author address: José M. Castanheira, CESAM, Department of Physics, University of Aveiro, 3810-193 Aveiro, Portugal.
E-mail: jcast@ua.pt

DOI: 10.1175/2008JAS2862.1

variations of the refractive properties of the lower stratospheric flow (e.g., Hartmann et al. 2000) or by downward reflection from higher stratospheric levels (Perlwitz and Harnik 2004). Other mechanisms include a downward progression of zonal mean anomalies via eddy–mean flow interaction (e.g., Eichelberger and Holton 2002). Song and Robinson (2004) suggested that when the downward-progressing zonal mean zonal circulation anomalies reach the tropopause, the response to stratospheric anomalies is amplified by eddy (i.e., wave) feedbacks. Wittman et al. (2007) proposed that changes of the vertical shear of the zonal mean zonal wind in the lower stratosphere modify the baroclinic instability in the tropospheric midlatitude jet. Tanaka and Tokinaga (2002) investigated the baroclinic instability of northern winter atmosphere considering a three-dimensional (3D) normal mode expansion of the global atmospheric circulation. Their results suggest a positive feedback mechanism in which the unstable baroclinic modes feed extra westerly momentum into the polar jet during strong polar vortex episodes.

Whatever the mechanism(s) for the downward progression of polar vortex anomalies (and one does not exclude the others), it is a well-established fact that strong vortex anomalies may progress downward and that zonal mean zonal wind anomalies may reach the lower troposphere at high latitudes.

The purpose of this study is twofold: (i) to analyze the 3D structure of baroclinic Rossby waves and the respective energy during periods of strong vortex accelerations or decelerations and (ii) to assess the sensitivity of the barotropic Rossby waves to the vortex strength. With regard to the first objective, it will be shown that rapid decelerations of the stratospheric vortex are forced by baroclinic Rossby wave bursts into the stratosphere, mainly of wavenumber 1, whereas rapid accelerations occur during times of diminished baroclinic Rossby wave propagation. Although these results may be taken as a classical view of stratospheric forcing, it is worth stressing that they were obtained based on a new diagnostic approach that allows obtaining a three-dimensional picture of the total (i.e., climatology + anomaly) Rossby waves during the diagnosed events. The method also allows us to identify the response (sensitivity) of the tropospheric (barotropic) Rossby waves to the strength of the stratospheric polar vortex. This aspect may be viewed as the main new contribution of this work; the obtained results suggest that the response is mediated by changes of the topographic forcing due to zonal mean zonal wind anomalies that progress downward from the stratosphere to the troposphere.

2. Data and method

a. Normal mode expansions

The data were obtained from the National Centers for Environmental Prediction–National Center for Atmospheric Research (NCEP–NCAR) reanalysis dataset (Kalnay et al. 1996) and we have used November to April daily means of the horizontal wind components (u, v) and of the geopotential height, available at 17 standard pressure levels from 1000 to 10 hPa, with a horizontal grid resolution of 2.5° latitude × 2.5° longitude. The data cover the period 1959–2006.

The horizontal wind (u, v) and geopotential height ϕ were expanded in terms of the normal modes of the NCEP–NCAR reference atmosphere (see Liberato et al. 2007 and references therein for details); that is,

$$\begin{bmatrix} u \\ v \\ \phi \end{bmatrix} = \sum_{m=0}^{\infty} \sum_{s=-\infty}^{\infty} \sum_{l=0}^{\infty} \sum_{\alpha=1}^{3} w_{msl}^{\alpha}(t) \times G_m(p)\ \exp(is\lambda)\,\mathbf{C}_m \cdot \begin{bmatrix} U(\theta) \\ iV(\theta) \\ Z(\theta) \end{bmatrix}_{msl,\alpha}, \quad (1)$$

where λ, θ, and p are the longitude, latitude, and pressure, respectively. The functions $G_m(p)$ represent separable vertical structures, and $\mathbf{C}_m = \mathrm{diag}[(gh_m)^{1/2}, (gh_m)^{1/2}, gh_m]$ is a diagonal matrix of scaling factors, with g representing the earth's gravity and h_m the equivalent heights. The vertical index $m = 0$ refers to the barotropic vertical structure and $m > 0$ refers to baroclinic vertical structures. Each horizontal structure function is given by the product of a zonal wave with wavenumber s and a vector $[U(\theta), iV(\theta), Z(\theta)]^{\mathrm{T}}_{msl,\alpha}$ that defines the meridional profile of the wave, where l is a meridional index that may be regarded as an indicator of the meridional scale of the motion. The index $\alpha = 1, 2, 3$ refers to westward-traveling inertio-gravity waves, Rossby waves, and eastward-traveling inertio-gravity waves, respectively. Figure 1 shows the first five vertical structure functions of the NCEP–NCAR atmosphere.

It may be shown that for $s \geq 1$, the total (i.e., kinetic + available potential) energy per unit area associated with a given mode is proportional to the squared norm of the respective expansion coefficient w_{msl}^{α} (Liberato et al. 2007 and references therein); that is,

$$E_{msl}^{\alpha}(t) = \frac{p_s h_m}{2} \left| w_{msl}^{\alpha}(t) \right|^2, \quad (2)$$

where the prescribed level of constant pressure near the earth's surface, $p_s = 1011.3$ hPa, represents the mean sea level pressure of the NCEP–NCAR reanalysis dataset.

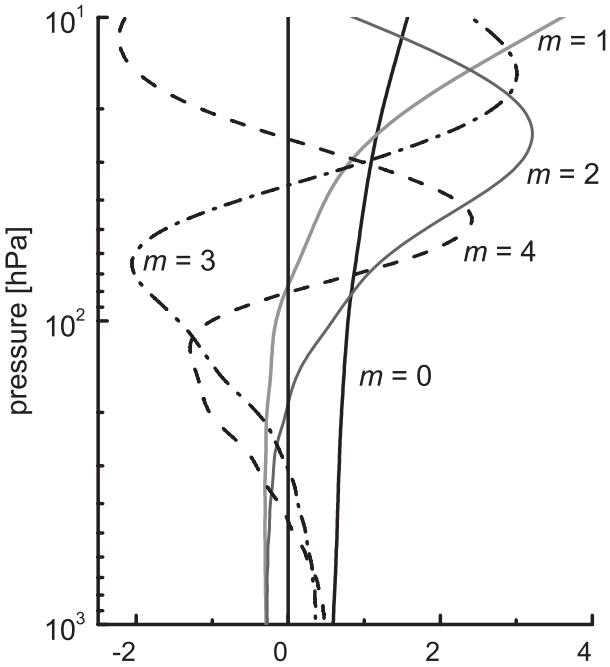

FIG. 1. Vertical structure functions of the barotropic $m = 0$ and the first four baroclinic modes ($m = 1,\ldots, 4$) of the NCEP–NCAR atmosphere.

The total energy associated with each Rossby or gravity wave characterized by a given vertical structure m and a given wavenumber s is obtained by summing the energy associated with all meridional indices l. Daily energy anomalies were obtained by subtracting the seasonal cycle, which was estimated by computing the multiannual mean for each calendar day and then smoothing the obtained time series of daily multiannual means with a 31-day running average.

b. Polar vortex strength

The polar vortex strength is represented by means of the stratospheric Northern Hemisphere annular mode (NAM) time series as computed by Baldwin and Dunkerton (2001). The NAM indices, covering the period 1958 to 2006, were obtained from the associated web page (http://www.nwra.com/resumes/baldwin/nam.php). A new index (hereafter referred to as the "slope index") was then defined as the time rate of change of the NAM time series at 50 hPa, which was previously smoothed by a 15-day running average. The slope index was used to identify periods of strengthening and periods of weakening of the stratospheric vortex. Events of strong accelerations (strengthening) or strong decelerations (weakening) of the stratospheric vortex were identified when the slope index was respectively above or below one standard deviation (std dev) of its mean value, during a period of at least 5 consecutive days. It may be noted that a shorter threshold of 3 consecutive days and a longer threshold of 7 consecutive days were also considered, but the obtained results remained qualitatively the same. It may be also noted that we have restricted the data to strong acceleration and to strong deceleration periods occurring before the final stratospheric warming to ensure that the considered periods remained in the stratospheric winter regime. As shown in Table 1, both the rapid deceleration periods and the rapid acceleration periods were stratified into three types according to the initial and final strength of the vortex. It may be noted that such classification of episodes based on vortex strength takes into account the possibility that the wave forcing of rapid decelerations may be different when the vortex is initially strong or when it is already in a weak state. The same reasoning applies to the cases of rapid acceleration in which the decreasing of wave forcing may also depend on the initial state of the vortex; that is, the strengthening of a vortex that is already strong may be different from the strengthening of a vortex that is initially weak. Finally, it is worth noting that all considered events are well separated in time; just two out of the 81 deceleration events are separated by 6 days, with the remaining ones being separated by at least 13 days; and the same happens in the case of almost all of the 117 acceleration events that are separated by at least 15 days, with only six cases presenting separation times between 8 and 14 days.

With the aim of assessing the sensitivity of barotropic Rossby waves to the vortex strength, we have also distinguished between two types of episodes: strong vortex episodes (SVEs) and weak vortex episodes (WVEs). For this purpose, the original daily NAM at 50 hPa was smoothed by an 11-day moving average, and SVEs (WVEs) were then defined as those periods when the smoothed vortex is one standard deviation above (below) the mean value during at least 15 days. It may be noted that our choice of an 11-day smoothing window was motivated by the fact that NAM anomalies take about 10 days to progress downward from the middle stratosphere to near the tropopause (Baldwin and Dunkerton 2001). However, it is worth noting that different smoothing windows and different minimum period lengths were tested but the obtained results remained virtually the same. We have also restricted the identification of SVEs and WVEs to the months of November to March to reduce the number of days after final stratospheric warmings.

c. Topographic Rossby wave model

We made use of the topographic Rossby wave model of Charney and Eliassen (1949) to illustrate how the barotropic waves may respond to changes in intensity of

TABLE 1. Classification of strong deceleration and strong acceleration events according to vortex strength. NAM-I and NAM-F refer to the initial and final vortex strength, respectively. Values of NAM-I (NAM-F) indicate thresholds that are surpassed at least once in the 15-day period before (after) the strong accelerations or decelerations begin (end). Upward (↑) and downward (↓) arrows indicate accelerations and decelerations of the vortex, respectively. The vortex strength is normalized to 1 std dev.

	Type A↓	Type B↓	Type C↓	Type D↑	Type E↑	Type F↑
NAM-1	> 1	> 0.5	< 0.5	< -1	< -0.5	> -0.5
NAM-F	> -0.5	< -0.5	< -1	< 0.5	> 0.5	> 1

the zonal mean zonal wind associated with the fluctuations in strength of the polar vortex. The model simply consists of a homogeneous fluid of variable depth, the upper boundary being located at a fixed height H and the lower boundary having variable height $h(x,y)$, where $|h| \ll H$. Considering the quasigeostrophic scaling on a β plane—$|\zeta_g| \ll f_0$ where ζ_g and f_0 are the geostrophic relative vorticity and the planetary vorticity, respectively—the barotropic vorticity equation linearized about a constant zonal flow U takes the form

$$\left(\frac{\partial}{\partial t} + U\frac{\partial}{\partial x}\right)\nabla^2\psi' + r\nabla^2\psi' + \beta\frac{\partial\psi'}{\partial x} = -f_0\frac{U}{H}\frac{\partial h}{\partial x}, \quad (3)$$

with

$$u'_g = -\frac{\partial\psi'}{\partial y}, \quad v'_g = \frac{\partial\psi'}{\partial x}, \quad \zeta'_g = \nabla^2\psi', \quad (4)$$

where $f_0 = 2\Omega\sin\varphi_0$ is the Coriolis parameter at the central latitude φ_0 of the β plane, $\beta = 2\Omega\cos\varphi_0/a$, and the perturbed geostrophic wind (u'_g, v'_g) and relative vorticity ζ'_g, are expressed in terms of the perturbation streamfunction ψ'. It may be noted that parameter r in Eq. (3) represents a linear damping of the relative vorticity because of the boundary layer drag, which is modeled in the form of Ekman pumping.

For steady flow, and assuming a topography of the form

$$h(x, y) = \Re[h_0 \exp(ikx)]\cos(ly), \quad (5)$$

where $\Re[\cdot]$ denotes "real part of", Eq. (3) has the following solution:

$$\psi'(x, y) = \Re[\psi'_0 \exp(ikx)]\cos(ly), \quad (6)$$

with the complex amplitude given by

$$\psi'_0 = \frac{f_0 h_0}{H(K^2 - K_s^2 - i\varepsilon)}, \quad (7)$$

where k and l are the zonal and meridional wavenumbers, respectively, and $K^2 = k^2 + l^2$ is the total horizontal wavenumber squared. The remaining parameters

$$K_s^2 = \frac{\beta}{U} \quad \text{and} \quad \varepsilon = \frac{rK^2}{kU} \quad (8)$$

account for the sensitivity of the complex wave amplitude to the zonal background flow.

3. Results

a. Wave forcing of the polar vortex

Figure 2 shows the obtained composites of the energy anomalies associated with the baroclinic Rossby waves of zonal wavenumbers $s = 1, 2, 3$, for the six considered types of events as defined in Table 1. Day 0 refers to the first day of each event and curves represent the sum of the energy associated with the first five baroclinic modes ($m = 1, 2, 3, 4, 5$). It may be noted that higher baroclinic modes ($m \geq 6$) have much smaller energy and were therefore neglected. In fact, by making composites of each baroclinic mode on an individual basis, it may be further observed that the main contribution for energy anomalies is provided by the vertical baroclinic modes $m = 1$ and 2, which have maximum amplitudes in the lower stratosphere (Fig. 1). Composites of the smoothed NAM, from which the slope index was derived, are also shown in Fig. 2. It is worth noting that rapid decelerations (accelerations) of the stratospheric vortex occur during strong positive (negative) anomalies of the energy associated with baroclinic Rossby waves, mainly of wavenumber 1; this feature clearly suggests that the forcing of vortex strength is performed by the baroclinic Rossby waves.

The 3D structure of the baroclinic Rossby waves of wavenumber 1 during rapid accelerations and rapid decelerations of the stratospheric vortex may be estimated using Eq. (1). Accordingly we have computed the composite wave for a period of 5 days centered at the day of maximum or at the day of minimum energy anomaly of wavenumber 1. Figures 3 and 4 show the obtained 3D structures of geopotential height of wavenumber 1 for deceleration events of type A and for acceleration events of type F (see Table 1). Structures similar to those of type A were also obtained for the other two types of deceleration events (i.e., types B and C); the same was observed in the case of the two other types of acceleration events (i.e., types D and E) that presented 3D wave structures very similar to those of type F. As shown in Fig. 3 (Fig. 4) the amplitude of the wave is large (small) during vortex decelerations (accelerations). Both

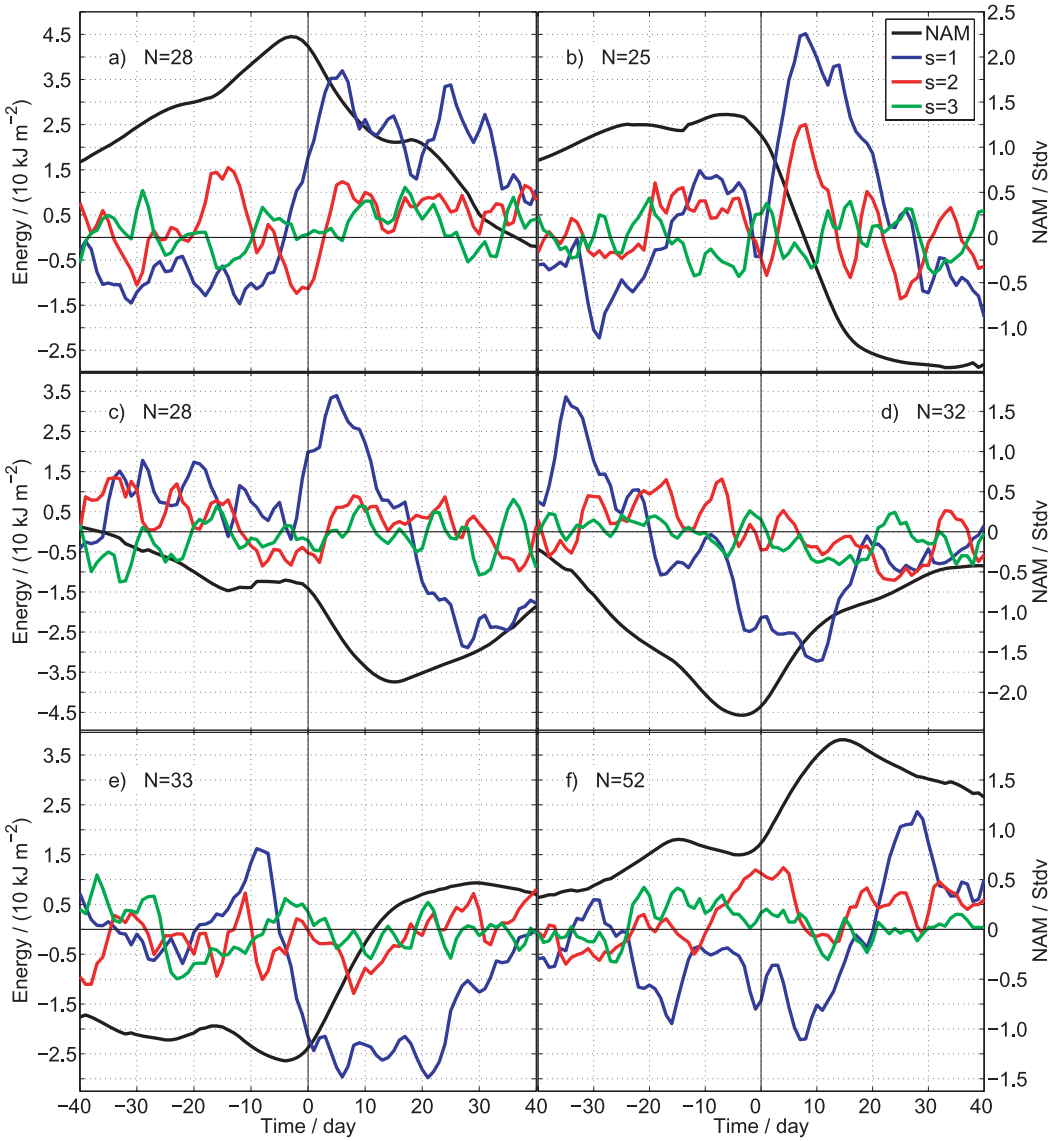

FIG. 2. Composites of the energy anomalies associated with baroclinic (m = 1, 2, 3, 4, 5) Rossby waves with wavenumbers s = 1, 2, 3 for the considered six types of (a)–(c) deceleration and (d)–(f) acceleration events (see Table 1). Black curves represent the time evolution of the composites of smoothed NAM at 50 hPa. Day zero refers to the first day of the acceleration or deceleration periods. Values of N indicate the number of events of each type.

composites of acceleration and deceleration events present a clear westward phase tilting with height that indicates upward energy propagation (upper left panels). However, the wave signal is confined to the northern high latitudes (upper right panels); during rapid vortex decelerations the wave amplitude maximum appears north of 60°N, being shifted a few degrees southward during rapid vortex accelerations. Finally it is worth stressing that in both deceleration and acceleration events (lower panels in Figs. 3 and 4), the waves present almost perfect out-of-phase patterns between 500 and 50 hPa.

b. Sensitivity of barotropic Rossby waves to the vortex strength

During strong vortex events, positive anomalies of the zonal mean zonal wind are observed northward of 45°N extending from the stratosphere to the lower troposphere (e.g., Hartmann et al. 2000, their Fig. 3)—a feature that is also clearly apparent in the patterns presented in Fig. 5, which shows the composites of the barotropic component of zonal mean zonal wind for SVEs and WVEs. Near the surface, the maximum wind

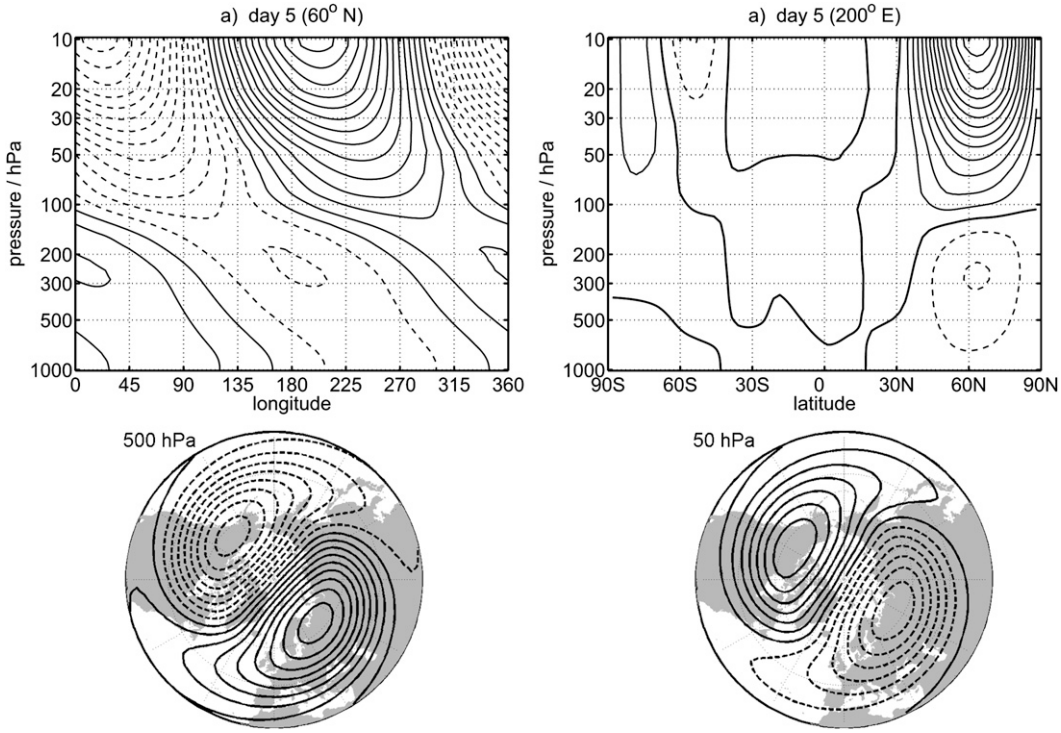

FIG. 3. Composite of the baroclinic (m = 1, 2, 3, 4, 5) Rossby wavenumber 1 for periods of 5 days centered at day 5 after the beginning of deceleration events of type A (see Table 1 and Fig. 2a). (top) Vertical cross sections at (left) 60°N and (right) 200°E with contour intervals of 50 gpm. (bottom) Horizontal structures at (left) 500 and (right) 50 hPa with contour intervals of 10 and 40 gpm, respectively.

anomalies are observed around 60°N (e.g., Limpasuvan et al. 2005, their Fig. 3). Using a primitive equation model linearized around a zonally symmetric basic state, Held and Ting (1990) showed increased amplitudes of orographically forced waves in response to changes in the zonal background flow. Because the vortex variability is associated with changes of the tropospheric zonal mean zonal wind, it is to be expected that vortex variability is also associated with changes in the topographic forcing of barotropic (m = 0) Rossby waves. Accordingly, the sensitivity of the barotropic Rossby waves to the vortex strength was assessed by computing the respective energy during strong and weak vortex events.

Table 2 (upper half) shows the mean energy anomalies of the barotropic (m = 0) and baroclinic (m = 1, 2, 3, 4, 5) modes of Rossby waves with wavenumbers $1 \leq s \leq 5$. The statistical significance level of anomalies is also indicated and was estimated by fixing the calendar dates of the events and then performing 10 000 random permutations of the 48 years. It may be observed that during SVEs (WVEs) the barotropic Rossby waves have more (less) energy than the mean. Energy anomalies of the barotropic waves are statistically significant at the 99% level (p = 0.01). Energy anomalies associated with baroclinic waves are not statistically significant, but it is worth noting that their values are negative, a result that is consistent with the fact that baroclinic positive energy anomalies occur during decelerations of the vortex (i.e., mainly during transitions between vortex states and not along a given persistent state of the vortex). Figure 6 (left panel) shows the wavenumber spectra of the energy differences (black solid line) and there is good evidence that the positive energy anomalies that are shown in Table 2 (upper half) are mainly due to the contributions of zonal wavenumbers 1 and 3, in strong contrast with wavenumber 2 that does not seem to be sensitive to the vortex strength.

The apparent lack of sensitivity of zonal wavenumber 2 to the vortex strength deserves further investigation. For this purpose we began by superimposing on the wave spectra of energy (Fig. 6, left) the amplitude of the Fourier components of the mean topography in the latitudinal band 55°–65°N. The minimum in amplitude of Fourier component s = 2 is worth emphasizing because this feature—together with the abovementioned fact that near the surface the maximum wind anomalies associated with stratospheric vortex anomalies are observed around 60°N—strongly suggests that the observed

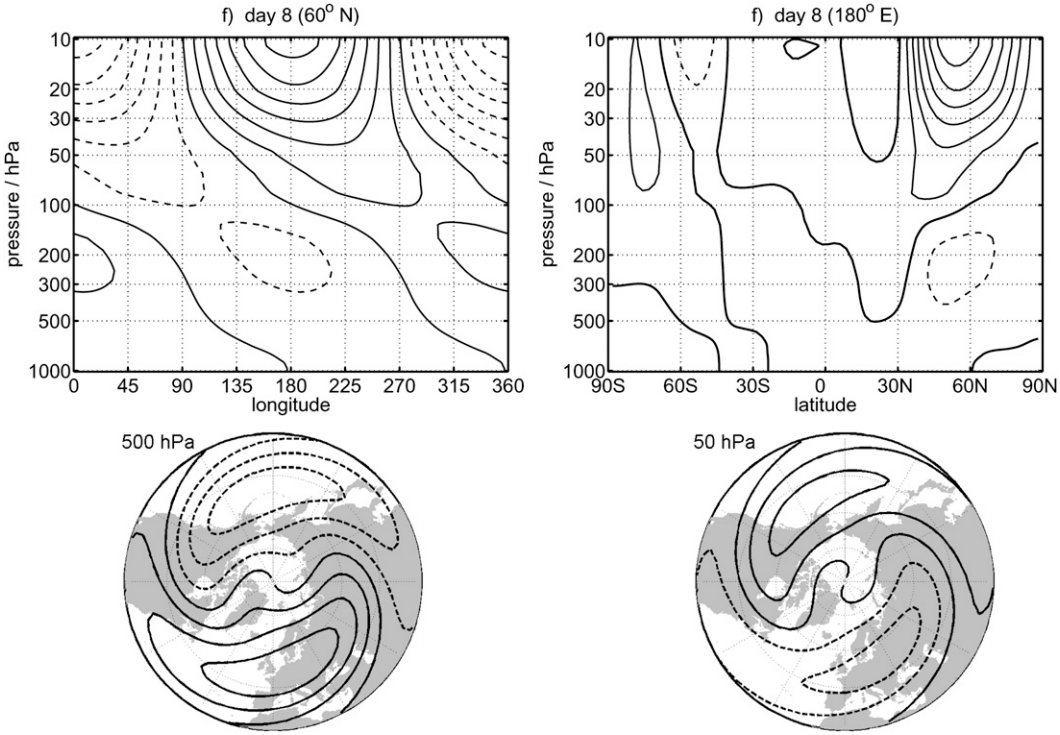

FIG. 4. As in Fig. 3, but with respect to the acceleration events of type F. The composite is centered at day 8 after the beginning of acceleration events (see Table 1 and Fig. 2f). (top) Vertical cross sections are at (left) 60°N and (right) 180°E.

insensitivity of wavenumber 2 to the vortex state may be due to the absence of a topographically induced response of zonal wavenumber 2 to changes in the zonal mean zonal wind.

The possibility that the response of the barotropic circulation to the vortex state is established via changes in the topographic forcing due to changes of the tropospheric zonal mean winds was therefore checked by assessing the sensitivity of the barotropic Rossby wave energy to the strength of the near-surface zonal wind. For this purpose we considered the time series of 850-hPa zonal mean zonal wind (U850) at 60°N and then identified strong (SU850) and weak (WU850) wind periods following the same procedure that was adopted in the identification of SVEs and WVEs. Accordingly, the original daily values of U850 were smoothed by an 11-day moving average and SU850 (WU850) episodes were defined as those periods when the smoothed zonal mean wind is one standard deviation above (below) the mean value during at least 15 days. Figure 6 (right) shows the lagged correlation between the vortex strength and U850, and despite the fact that both time series were smoothed by an 11-day running mean, it is well apparent that the vortex strength leads the U850 strength by about 4 days. Table 2 (lower half) also shows the mean energy anomalies of the barotropic and baroclinic Rossby waves during SU850 and WU850 periods. Obtained results clearly show that the sensitivity of barotropic Rossby wave energy to U850 strength is similar to the

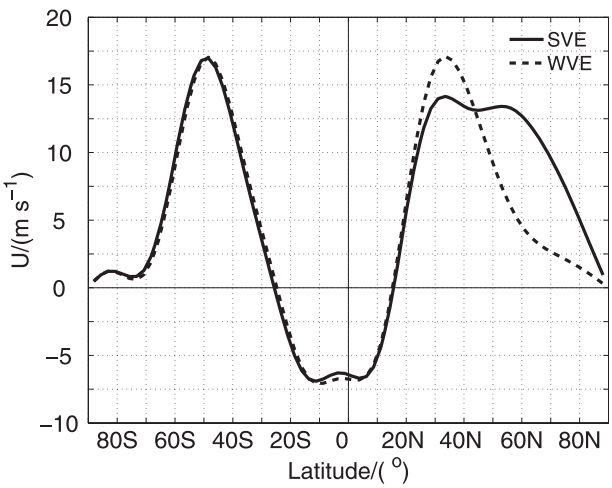

FIG. 5. Composites of the barotropic component of zonal mean zonal wind for strong and weak vortex events. The barotropic component has been rescaled to represent a vertical average weighted by the vertical structure function $G_0(p)$.

TABLE 2. Mean energy anomalies (10^7 J m^{-2}) of the barotropic ($m = 0$) and baroclinic ($m = 1, 2, 3,4, 5$) modes of Rossby waves with zonal wavenumbers $1 \leq s \leq 5$, during SVEs and WVEs, as well as during strong (SU850) and weak (WU850) 850-hPa zonal mean zonal wind episodes at 60°N. One, two, and three asterisks indicate values that are statistically significant at the 94%, 97.5%, and 99% levels, respectively. All remaining anomalies are statistically significant at levels below 85%.

	$m = 0$	$m = 1, 2, 3, 4, 5$
SVE	1.14***	−0.23
WVE	−1.18***	−0.44
SU850	0.69*	0.44
WU850	−1.29***	−1.00**

found sensitivity to vortex strength. However, the energy of the baroclinic Rossby waves appears to also be sensitive to U850 strength, a feature that may be viewed as resulting from the delayed changes of U850 relative to the changes of the vortex strength. In fact, while the vortex strength decelerates U850 may still remain strong; therefore, positive anomalies of the baroclinic Rossby wave energy may occur during strong U850. During WU850 episodes, negative anomalies of the baroclinic Rossby wave energy occur, leading to a fast recovery of the vortex strength. As shown in Fig. 6 (left), the spectrum of the barotropic energy differences between SU850 and WU850 periods (dashed black line) is very similar to the one of differences between SVEs and WVEs (solid black line) that has been previously discussed. It is therefore likely that the sensitivity of the barotropic wave energy to the vortex state is mediated by changes of topographic forcing resulting from changing tropospheric winds.

To gain some physical insight into the mechanism by which the barotropic waves may respond to the strength of the polar vortex, an analytical study was performed using the simple topographic Rossby wave model described in section 2. For this purpose, we have used Eq. (7) to compute the amplitudes of the steady wave solutions of Eq. (3), having considered the x-dependence of the height h of the lower boundary as given by the mean topography in the latitudinal band 55°–65°N and having set the remaining parameters according to the original study as given in Holton (2004, section 7.7.2). Figure 7 shows the squared amplitude of the wave solution of the model (which is proportional to the wave energy) as a function of the zonal-mean zonal background flow. It is well apparent that waves with zonal wavenumbers 1 and 3 are those that present more sensitivity to fluctuations in zonal mean zonal wind intensity, which is a result in close agreement with the above-obtained one in the case of the energy of barotropic waves (Fig. 6). However, it may be noted that the barotropic model represents an oversimplified view of the atmospheric circulation and that a fixed meridional wavenumber was used when evaluating Eq. (7). Accordingly, any result beyond the obtained qualitative agreement between model and observations is not to be expected, given the limitations implied by the a priori simplifications.

c. *SVE and WVE composites of the barotropic geopotential field*

Results presented in Figs. 6 and 7 clearly show that the barotropic Rossby waves with wavenumbers 1 and 3 are the more sensitive to deep changes in the vortex

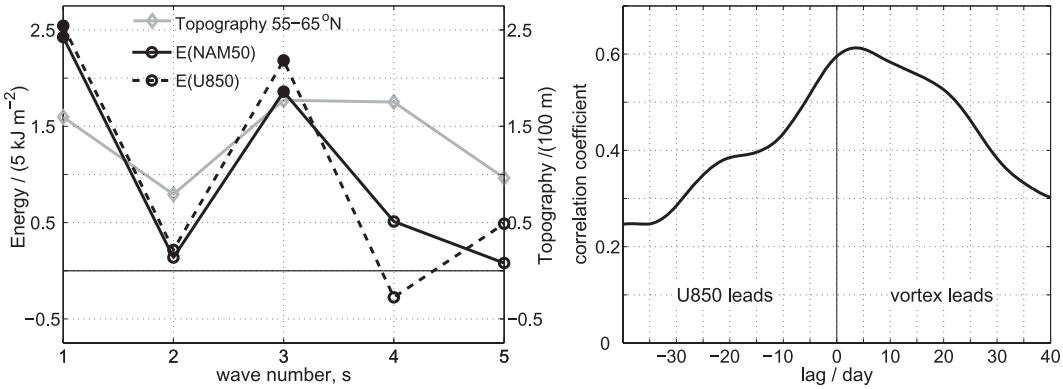

FIG. 6. (left) Wavenumber spectra of energy differences associated with barotropic Rossby waves between composites for strong and weak vortex events (i.e., SVE − WVE; solid black curve) and between strong (SU850) and weak (WU850) 850-hPa zonal mean zonal wind (U850) (i.e., SU850 − WU850; dashed black curve). Solid circles indicate energy differences that are statistically significant at the 99% level; the amplitude of the Fourier components of the mean topography in the 55°–65°N latitudinal band are also represented (gray curve). (right) Lagged correlations between vortex strength and U850; only NAM anomalies above or below one standard deviation were considered. Positive lags indicate that the vortex strength is leading.

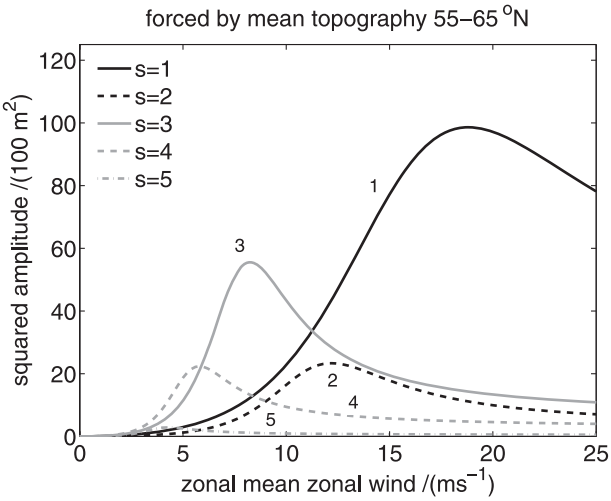

FIG. 7. Squared amplitudes of topographic waves as computed by the model of Charney and Eliassen [Eq. (7)] forced with the Fourier components of the mean topography in the latitudinal band 55°–65°N.

strength and strongly suggest that their sensitivity is due to topographic forcing. It is therefore to be expected that the tropospheric anomalies associated with changes in the vortex strength will strongly project on zonal wavenumbers 1 and 3. Figure 8 presents a set of composites respecting to strong and weak vortex events. The first, second, and third lines of Fig. 8 refer respectively to composites that were built using the zonal mean plus Rossby waves with zonal wavenumbers 1 and 3, using the Rossby wave with zonal wavenumber 2 alone, and using the zonal mean plus Rossby waves with zonal wavenumbers 1, 2, and 3. The first and the second columns respectively refer to composites for SVEs and WVEs, whereas the third column represents the respective differences (i.e., SVE − WVE). It may be noted that the barotropic component has been rescaled to represent the vertical average of the geopotential of isobaric levels weighted by the product of the mass density and the vertical structure function $G_0(p)$. Although the geopotential seasonal cycle was not removed before computing the difference between composites, similar difference patterns would be obtained using deseasonalized composites.

When the zonal mean and Rossby waves with zonal wavenumbers 1 and 3 are used to build the composites (Fig. 8, first row), it may be observed that the difference pattern is clearly dominated by zonally symmetric anomalies located at high latitudes and by well-developed wavy anomalies over the midlatitudes. As in the case of the Arctic Oscillation (AO) pattern (Thompson and Wallace 1998), there is a dipolar structure over the Atlantic Ocean but not over the central Pacific. Two other highs may be observed over the western border of North America and over the eastern border of Eurasia. The dipole over the Atlantic pattern reflects the known relationship between the fluctuations of the vortex strength and the intensity of the North Atlantic Oscillation (NAO). However, the high that is centered over the west coast of North America does not show up when tropospheric circulation is regressed onto the strength of the polar vortex (Castanheira et al. 2008, their Fig. 2). It may therefore be concluded that wavenumbers 1 and 3 are not able to capture the full linear relationship with the vortex strength.

Composites of barotropic geopotential fields that were built using Rossby waves with zonal wavenumber 2 alone (Fig. 8, second row) reveal clear differences between the patterns associated with strong and weak vortex events. This is especially conspicuous in the composite of differences and indicates that the role of wavenumber 2 cannot be neglected. In fact, although the energy of Rossby waves of zonal wavenumber 2 does not show any significant sensitivity to changes of vortex strength (see Fig. 6), this does not prevent these waves from being sensitive both in their phases and meridional structures. Several processes may have contributed to the observed changes in the pattern of wavenumber 2, such as wave–wave interactions and/or changes in the subtropical jet (see Fig. 5) associated with changes in the topographic- and heating-related forcing fields. The study of such processes is, however, beyond the scope of this work.

Composites of barotropic geopotential fields that were built using the zonal mean and Rossby waves with zonal wavenumbers 1, 2, and 3 (Fig. 8, third row) reveal similar structures to those retrieved with the zonal mean and Rossby waves with wavenumbers $s = 1$ and 3 (Fig. 8, first row). The difference pattern shows again a high degree of zonal symmetry at high latitudes and a wavy pattern may be observed over the midlatitudes. However, the pattern of differences shows two dipolar structures, one over each ocean basin, but the one located over the Atlantic basin presents a high center of much greater amplitude. It is also worth noting that the difference pattern represents characteristics of the Arctic Oscillation pattern.

A final aspect that deserves to be investigated relates to the possible nonlinear response of tropospheric circulation to stratospheric polar vortex changes, the nonlinearity being given by parameters K_s and ε in Eq. (7). In fact, the results presented in Fig. 7 clearly suggest that each wavenumber responds to topographic forcing in different ranges of the zonal mean zonal wind. For instance, wavenumbers 3 and 4 show large variations of squared amplitude for zonal mean winds in the range of

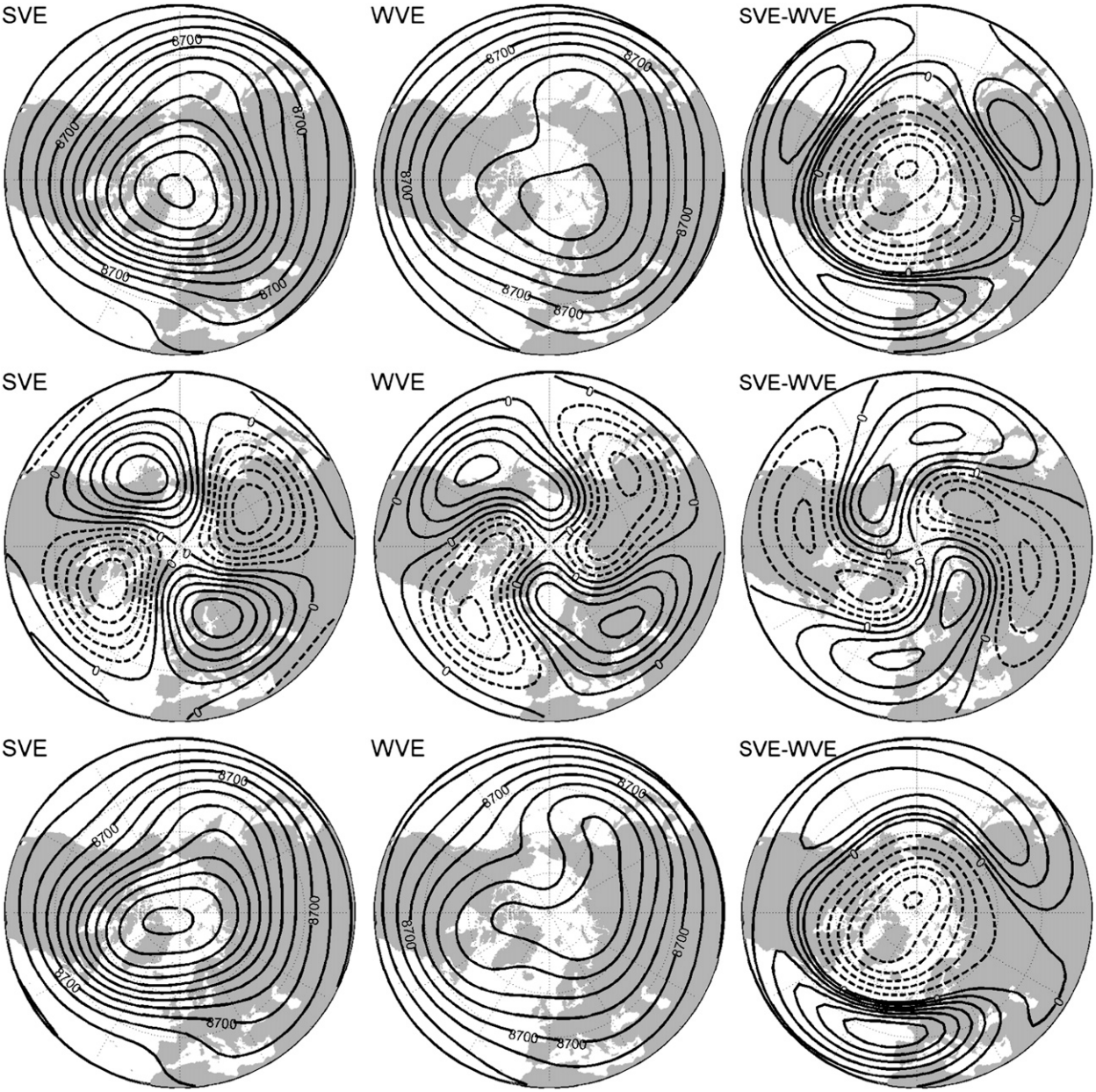

FIG. 8. Composites of barotropic geopotential fields for SVEs, WVEs, and the respective differences (SVE − WVE). Composites were built using (first row) the zonal mean plus Rossby wavenumbers $s = 1$ and 3, (second row) only Rossby wavenumber $s = 2$, and (third row) the zonal mean plus Rossby wavenumbers $s = 1, 2, 3$. At the first and third rows, the contour interval is 75 gpm for both SVE and WVE patterns, whereas for SVE − WVE the contour interval is 15 gpm for positive contours and 50 gpm for negative contours. In the case of zonal wavenumber 2 (second row), the contour interval is 15 gpm for both SVE and WVE patterns and 10 gpm in the case of SVE − WVE.

[0, 10] m s^{-1}, in contrast with wavenumbers 1 and 2, for which the largest variations of squared amplitude are observed for zonal mean winds greater than 10 m s^{-1}. It may therefore be possible that zonal wavenumber 3 does not respond to the strengthening of the vortex when it is already strong. To test this possibility, we have classified strong vortices into two types and have defined a moderately strong vortex (MSV) when its strength is in the range [0.25, 0.75] std dev and a very strong vortex (VSV) when its strength is above 1.25 std dev of the respective mean. Figure 9 shows the obtained composites of the difference (VSV − MSV) between the spectra of the energy of the barotropic Rossby waves for the two types of strong vortex. It may be noted that only zonal

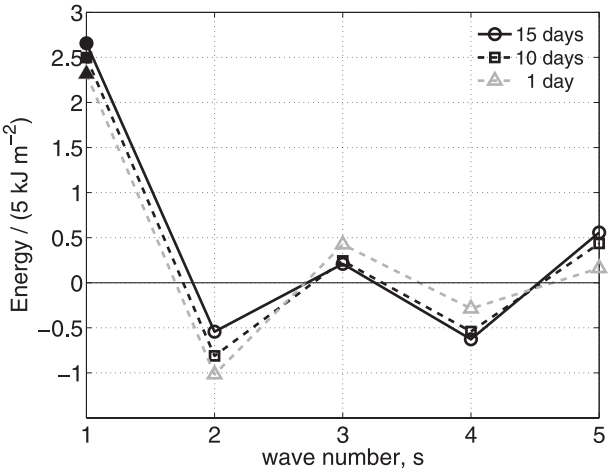

FIG. 9. Composite spectra of the differences between the means of the energy anomalies associated with barotropic Rossby waves during very strong (VSV) and moderately strong vortex (MSV) episodes (i.e., VSV − MSV). Circles, squares, and triangles identify obtained differences for episodes that lasted at least 15, 10, and 1 day(s), respectively. Solid symbols indicate energy differences that are statistically significant at the 99% level ($p = 0.01$), using a two-sided test.

wavenumber 1 presents statistically different ($p = 0.01$) values for the associated energy, and it is worth referring to the fact that obtained differences are even slightly greater than the difference obtained for SVE − WVE. In turn, the difference of the energy associated with zonal wavenumber 3 is close to zero and smaller than the absolute value of the energy associated with zonal wavenumber 2. Obtained results are therefore in strong agreement with what is to be theoretically expected from Eq. (7) (see Fig. 7). Finally, it may be noted that obtained results remain qualitatively the same when using different thresholds for episode duration. This is well apparent in Fig. 9, which shows the obtained energy differences between VSV and WSV episodes using thresholds of 1, 10, and 15 days.

The upper row in Fig. 10 presents composites of the difference between very strong and moderately strong vortices (i.e., VSV − MSV) when the barotropic geopotential field is built using wavenumbers (left) $s = 1$ and 2 or (right) $s = 1, 2$, and 3. It may be noted that the zonal mean was not included in the composites. The lower row in Fig. 10 shows similar composites but for the differences between strong and weak vortex events (i.e., SVE − WVE). The most prominent feature that may be observed in all composite differences is the dipolar structure over the Atlantic Ocean. However, when comparing the corresponding maps in the upper and lower rows, there is a clear eastward phase shift of the high-latitude wave pattern in the case of VSV − MSV that leads to a more meridional orientation of the North Atlantic dipole. In the case of SVE − WVE, the dipole presents a northwest–southeast tilting in agreement with the results of Castanheira et al. (2002), and it is worth noting that zonal wavenumber 3 seems to be the major contributor for such tilting. This feature may be understood by recalling that both the observed (Fig. 9) and the theoretical (Fig. 7) results point out that the variability of stationary Rossby wavenumber 3 is reduced when considering the strengthening of a zonal mean wind that is already strong. In fact, zonal wavenumber 3 seems to play a minor role in the composites of the upper row in Fig. 10. This minor role of wavenumber 3 sheds new light on the results of Castanheira and Graf (2003) that obtained a meridional dipole orientation of the NAO pattern when partitioning the data between SVE and WVE. These authors have also shown that the NAO correlation pattern presented a more zonal extension during strong polar vortex. Similar results were obtained by Kodera and Kuroda (2005) with regard to the zonal extension of the NAO correlation pattern. Calculating separately the correlation NAO patterns for high and low solar activity phases, Kodera and Kuroda (2005) found a more zonally extending pattern during the phase of high solar activity (see their Fig. 3). Their results agree with ours because the stratospheric vortex is stronger during high solar activity. The reduction of the variability of the barotropic Rossby waves of zonal wavenumber 3 during strong vortex episodes may therefore be the reason for the abovementioned differences in the zonal extension of the NAO dipole.

4. Concluding remarks

An analysis was performed on the dynamical coupling between the variability of the extratropical stratospheric and tropospheric circulations during the Northern Hemisphere winter. The global atmospheric circulation fields were expanded in terms of 3D normal modes of the NCEP–NCAR reanalyzed atmosphere. This expansion allows us both to separate the atmospheric circulation between Rossby and inertio-gravity waves and to identify their barotropic and baroclinic vertical structures.

The results give clear evidence as to the existence of a troposphere–stratosphere wave-driven coupled variability. On one hand, the vortex variability is forced by baroclinic Rossby wave bursts; on the other hand, there is a response of the barotropic Rossby waves to the vortex state. Although the forcing by baroclinic Rossby wave activity is not a new result in itself, the methodology adopted was able to provide a new confirmation of the dynamical theory of vortex variability: whereas radiative forcing always drives the vortex to a strong state,

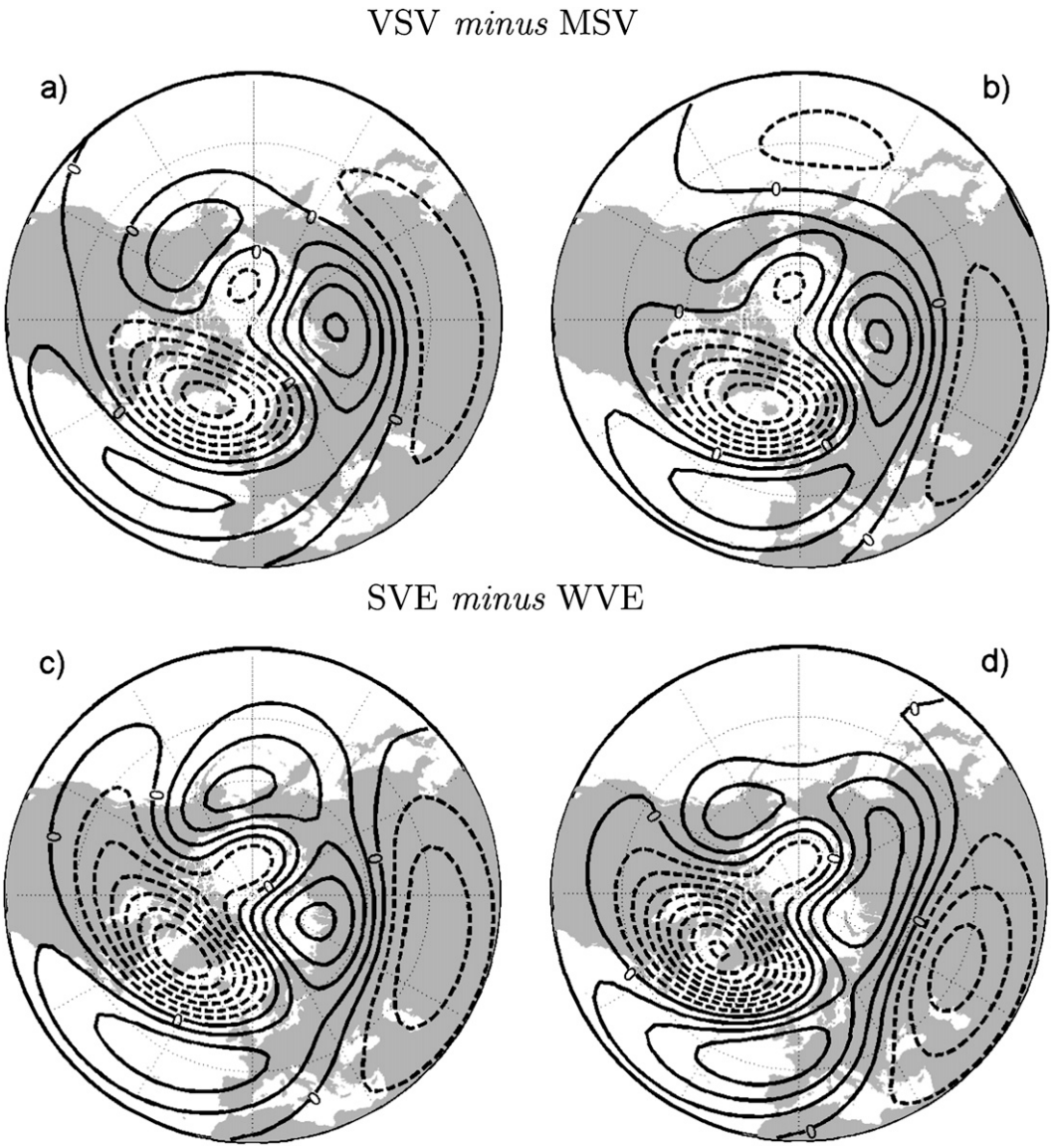

FIG. 10. Composite differences of barotropic geopotential waves (a),(b) between very strong and moderately strong vortices (i.e., VSV − MSV) and (c),(d) between strong and weak vortex events (i.e., SVE − WVE). Composites were built using wavenumbers $s = 1, 2$ for (a) and (c); and wavenumbers $s = 1, 2, 3$ for (b) and (d). Contour interval is 15 gpm.

baroclinic Rossby wave forcing is sometimes stronger than radiative forcing, leading to deceleration, and sometimes it is weaker than the mean, leading to acceleration. With regard to the response of the barotropic Rossby waves to the vortex state, strong evidence is presented that such response is mediated by changes of the topographic forcing due to zonal mean zonal wind anomalies progressing downward from the stratosphere.

Composites of differences of the barotropic circulation between strong and weak vortex states present patterns that are dominated by zonally symmetric anomalies at high latitudes and wavy anomalies at midlatitudes. This result is in close agreement with the findings by Castanheira et al. (2007, 2008), which show that zonally symmetric coherent variability is detected at high latitudes. In turn, the topographic ''reaction'' to such fluctuations in the strength of high-latitude zonal mean zonal wind induces a response of the tropospheric circulation to the vortex variability. The stationary barotropic Rossby waves with zonal wavenumbers 1 and 3 are the ones that have shown to be sensitive to the vortex state. The same zonal numbers are incidentally

those where the Fourier components of the mean topography in the latitudinal band 55°–65°N present maximum amplitudes.

Using the simple topographic wave model of Charney and Eliassen (1949), we have provided an analytical demonstration that the wave response to zonal mean zonal wind fluctuations is nonlinear. Results of performed analysis show that the barotropic Rossby waves of zonal wavenumber 3 respond to the strengthening of the zonal mean wind if it is initially weak but do not respond to the wind strengthening if the wind is already strong.

It was finally shown that changes of barotropic long ($s \leq 3$) Rossby waves associated with vortex variability reproduce an NAO-like dipole over the Atlantic Ocean, but no dipole is formed over the Pacific Ocean. It is suggested that the nonlinear wave response to topographic forcing may explain the spatial changes of the NAO correlation patterns that was found in previous studies (Castanheira and Graf 2003; Kodera and Kuroda 2005).

Overall, obtained results of the present study provide strong evidence that in addition to the known fact that vertical propagation of (baroclinic) Rossby waves is nonlinearly influenced by the zonal mean zonal wind (Charney and Drazin 1961), topographic forcing constitutes another important mechanism by which nonlinearity is introduced in the troposphere–stratosphere wave-driven coupled variability.

Acknowledgments. In this research, Dr. Laura de La Torre and Margarida L. R. Liberato have been supported by the grants SFRH/BPD/26474/2005 and SFRH/BD/32640/2006 of the FCT (Fundação para a Ciência e a Tecnologia, Portugal), respectively.

REFERENCES

Baldwin, M. P., and T. J. Dunkerton, 2001: Stratospheric harbingers of anomalous weather regimes. *Science,* **294,** 581–584.

Castanheira, J. M., and H.-F. Graf, 2003: North Pacific–North Atlantic relationships under stratospheric control? *J. Geophys. Res.,* **108,** 4036, doi:10.1029/2002JD002754.

——, ——, C. C. DaCamara, and A. Rocha, 2002: Using a physical reference frame to study global circulation variability. *J. Atmos. Sci.,* **59,** 1490–1501.

——, M. L. R. Liberato, C. A. F. Marques, and H.-F. Graf, 2007: Bridging the annular mode and North Atlantic Oscillation paradigms. *J. Geophys. Res.,* **112,** D19103, doi:10.1029/2007JD008477.

——, ——, L. de la Torre, H.-F. Graf, and A. Rocha, 2008: Annular versus nonannular variability of the Northern Hemisphere atmospheric circulation. *J. Climate,* **21,** 3180–3190.

Charney, J. G., and A. Eliassen, 1949: A numerical method for predicting the perturbations of the middle latitude westerlies. *Tellus,* **1,** 38–54.

——, and P. G. Drazin, 1961: Propagation of planetary-scale disturbances from the lower into the upper atmosphere. *J. Geophys. Res.,* **66,** 83–109.

Eichelberger, S. J., and J. R. Holton, 2002: A mechanistic model of the northern annular mode. *J. Geophys. Res.,* **107,** 4388, doi:10.1029/2001JD001092.

Hartmann, D. L., J. M. Wallace, V. Limpasuvan, D. W. J. Thompson, and J. R. Holton, 2000: Can ozone depletion and global warming interact to produce rapid climate change? *Proc. Natl. Acad. Sci. USA,* **97,** 1412–1417.

Haynes, P., 2005: Stratospheric dynamics. *Annu. Rev. Fluid Mech.,* **37,** 263–293, doi:10.1146/annurev.fluid.37.061903.175710.

Held, I. M., and M. Ting, 1990: Orographic versus thermal forcing of stationary waves: The importance of the mean low-level wind. *J. Atmos. Sci.,* **47,** 495–500.

Holton, J. R., 2004: *An Introduction to Dynamic Meteorology*. 4th ed. Academic Press, 535 pp.

Kalnay, E., and Coauthors, 1996: The NCEP/NCAR 40-Year Reanalysis Project. *Bull. Amer. Meteor. Soc.,* **77,** 437–471.

Kodera, K., and Y. Kuroda, 2005: A possible mechanism of solar modulation of the spatial structure of the North Atlantic Oscillation. *J. Geophys. Res.,* **110,** D02111, doi:10.1029/2004JD005258.

Liberato, M. L. R., J. M. Castanheira, L. de la Torre, C. C. DaCamara, and L. Gimeno, 2007: Wave energy associated with the variability of the stratospheric polar vortex. *J. Atmos. Sci.,* **64,** 2683–2694.

Limpasuvan, V., D. L. Hartmann, D. W. J. Thompson, K. Jeev, and Y. L. Yung, 2005: Stratosphere–troposphere evolution during polar vortex intensification. *J. Geophys. Res.,* **110,** D24101, doi:10.1029/2005JD006302.

Perlwitz, J., and N. Harnik, 2004: Downward coupling between the stratosphere and troposphere: The relative roles of wave and zonal mean processes. *J. Climate,* **17,** 4902–4909.

Song, Y., and W. A. Robinson, 2004: Dynamical mechanisms for stratospheric influences on the troposphere. *J. Atmos. Sci.,* **61,** 1711–1725.

Tanaka, H. L., and H. Tokinaga, 2002: Baroclinic instability in high latitudes induced by polar vortex: A connection to the Arctic Oscillation. *J. Atmos. Sci.,* **59,** 69–82.

Thompson, D. W., and J. M. Wallace, 1998: The Arctic Oscillation signature in the wintertime geopotential height and temperature fields. *Geophys. Res. Lett.,* **25,** 1297–1300.

Wittman, M. A., A. J. Charlton, and L. M. Polvani, 2007: The effect of lower stratospheric shear on baroclinic instability. *J. Atmos. Sci.,* **64,** 479–496.